PHOTONICS Research

Characterization of Yb-doped ZBLAN fiber as a platform for radiation-balanced lasers

Mostafa Peysokhan,[1,2] Esmaeil Mobini,[1,2] Arman Allahverdi,[2,3] Behnam Abaie,[1,2] and Arash Mafi[1,2,*]

[1]Department of Physics and Astronomy, University of New Mexico, Albuquerque, New Mexico 87131, USA
[2]Center for High Technology Materials, University of New Mexico, Albuquerque, New Mexico 87106, USA
[3]Department of Electrical and Computer Engineering, University of New Mexico, Albuquerque, New Mexico 87131, USA
*Corresponding author: mafi@unm.edu

Received 14 October 2019; revised 11 December 2019; accepted 11 December 2019; posted 13 December 2019 (Doc. ID 380615); published 31 January 2020

Recent advances in power scaling of fiber lasers are hindered by the thermal issues, which deteriorate the beam quality. Anti-Stokes fluorescence cooling has been suggested as a viable method to balance the heat generated by the quantum defect and background absorption. Such radiation-balanced configurations rely on the availability of cooling-grade rare-earth-doped gain materials. Herein, we perform a series of tests on an ytterbium-doped ZrF_4–BaF_2–LaF_3–AlF_3–NaF (ZBLAN) optical fiber to extract its laser-cooling-related parameters and show that it is a viable laser-cooling medium for radiation balancing. In particular, a detailed laser-induced modulation spectrum test is performed to highlight the transition of this fiber to the cooling regime as a function of the pump laser wavelength. Numerical simulations support the feasibility of a radiation-balanced laser, but they highlight that practical radiation-balanced designs are more demanding on the fiber material properties, especially on the background absorption, than solid-state laser-cooling experiments.

https://doi.org/10.1364/PRJ.380615

1. INTRODUCTION

Fiber lasers are attractive sources of high-power coherent radiation for industrial and directed energy applications. They have many excellent properties; for example, they enjoy high power efficiencies, broad gain linewidths, and diffraction-limited beam qualities. Moreover, the availability of fully fiberized cavities without the need for precise alignment makes them quite flexible for implementation outside the controlled environment of research laboratories [1,2]. Efficient heat mitigation plays an important role in the quest to achieve ever-increasing output powers from fiber lasers and amplifiers. Current approaches to power scaling are limited by the thermally induced mode instability, which degrades the output beam quality [3–7]. Anti-Stokes fluorescence (ASF) cooling has been suggested as a viable method to address such thermal issues [8,9]. In practical designs, ASF cooling can reduce the heat-load or even balance the heat generated by the quantum defect and background absorption, which is dubbed as radiation balancing [10–13].

The development of a viable radiation-balanced Yb-doped fiber laser depends on the synthesis of a high-purity cooling-grade glass host. At this point, the most viable material to demonstrate the concept of a radiation-balanced laser (RBL) in an optical fiber platform is the Yd-doped ZBLAN (ZrF_4–BaF_2–LaF_3–AlF_3–NaF) glass, because it has been successfully cooled via ASF [8]. It also has interesting properties for certain specialized high-power applications, especially because ZBLAN can be doped with a higher Yb concentration than silica glass [14]. The relatively small quantum defect of Yb dopants, high doping concentration, wide pump absorption band, availability of low-cost and high-brightness pump diodes in the 0.9–1.0 μm absorption band of Yb, and the possibility of making a double-cladding fiber configuration make Yb-doped ZBLAN fibers an attractive choice for fiber RBL operation [15–19].

In the quest to develop a viable radiation-balanced fiber laser or amplifier, it is important to fully characterize the optical (gain and absorption) and ASF cooling properties of Yb-doped ZBLAN glass fibers. In particular, the wavelength dependence of the ASF cooling efficiency is needed for choosing the optimal pump and laser wavelengths. Moreover, it has been shown that the heat generation due to the parasitic absorption of the host glass plays an important role in setting the thermal behavior of a high-power fiber laser system and that it can even dominate the heat generation due to the quantum defect [20]. Therefore, it is critical to accurately determine the parasitic absorption of Yb-doped ZBLAN glass fibers. In this paper, we combine two techniques: the laser-induced modulation spectrum (LITMoS) test developed in Sheik-Bahae's research group [21], and our

recently developed measuring the absorption coefficient via side-light analysis (MACSLA) method [22] to characterize the cooling efficiency of a cooling-grade Yb-doped ZBLAN glass fiber as a function of the wavelength and determine its resonant and parasitic absorption properties. We will then use the extracted parameters to explore the design and optimization of an Yb-doped ZBLAN glass fiber laser system.

To quantify the ASF cooling, it is common to use the cooling efficiency, η_c, whose determination is a primary focus of this paper. In a conventional laser-cooling setup, where the material is pumped by a laser at frequency ν_p and cooled via ASF, η_c is the net power density (per unit volume) extracted from the material (P_{net}) per unit power density absorbed or scattered (P_{abs}): $\eta_c = P_{\text{net}}/P_{\text{abs}}$. It can be shown that the cooling efficiency can be written as

$$\eta_c(\lambda_p) = \frac{\lambda_p}{\lambda_f}\eta_q\eta_{\text{abs}}(\lambda_p) - 1, \tag{1}$$

where the absorption efficiency is given by

$$\eta_{\text{abs}}(\lambda_p) = \frac{\alpha_r(\lambda_p)}{\alpha_r(\lambda_p) + \alpha_b}. \tag{2}$$

$\alpha_r(\lambda_p)$ is the resonant pump absorption coefficient, and α_b is the parasitic background absorption coefficient. λ_f is the mean fluorescence wavelength, η_q is the external quantum efficiency, and $\eta_{\text{abs}}(\lambda_p)$ is the absorption efficiency at the pump wavelength $\lambda_p = c/\nu_p$ (c is the speed of light in vacuum). We present a derivation of Eq. (1) in Appendix A, but for here, it is sufficient to know that $0 \le \eta_q \le 1$ and $0 \le \eta_{\text{abs}} \le 1$.

It must be noted that the wavelength dependence of the fiber temperature drop has been previously explored in several laser-cooling experiments [15–18]; however, in this work, we focus on determining the wavelength dependence of the cooling efficiency, η_c, and extract the key parameters for designing a radiation-balanced laser, i.e., the parasitic background absorption coefficient, the resonant pump absorption coefficient, as well as the quantum efficiency of the cooling medium. For ASF cooling, P_{net} must be positive (net heat extraction), which is equivalent to a positive value for the cooling efficiency, η_c. From Eq. (1), one can immediately determine that $\lambda_f < \lambda_p$ is a necessary condition for ASF cooling, given that $0 \le \eta_q, \eta_{\text{abs}} \le 1$. In practice, both η_q and η_{abs} must be very close to unity to observe ASF cooling. The reason is that λ_p cannot be much longer than λ_f; otherwise the resonant pump absorption coefficient, $\alpha_r(\lambda_p)$, would become too small, hence lowering the value of the absorption efficiency $\eta_{\text{abs}}(\lambda_p)$ [see Eq. (2)]. Therefore, in an ASF cooling experiment, λ_p/λ_f [$\eta_{\text{abs}}(\lambda_p)$] is a monotonically increasing (decreasing) function of the pump wavelength; it is the balance between λ_p/λ_f and $\eta_{\text{abs}}(\lambda_p)$ if $\eta_q \approx 1$, which dictates an ASF cooling range in λ_p. In the following, we will use the LITMoS test and measure the wavelength dependence of η_{abs}, which allows us to determine η_q and η_{abs} for the cooling-grade fiber. Once η_{abs} is determined, we will then apply the MACSLA method to find the values of the parasitic absorption α_b, as well as $\alpha_r(\lambda_p)$.

2. WAVELENGTH DEPENDENCE OF THE COOLING EFFICIENCY

The experimental setup to perform the LITMoS test and measure the wavelength dependence of the cooling efficiency whose is depicted in Fig. 1. All the measurements are done for a multimode (1% YbF_3) ZBLAN fiber with the core diameter of 300 μm and cladding diameter of 430 μm. Both facets of the fiber are polished with the cooling-grade polishing technique that is detailed in Appendix B. Per Fig. 1(a), the ZBLAN fiber is pumped from the left-side by a tunable Ti:sapphire laser, which is coupled to the ZBLAN fiber via a 20× microscope objective. The pump is reflected back into the fiber by an objective–mirror combination in a double-pass configuration. The fiber temperature is measured by a thermal camera, which is placed on top of the ZBLAN fiber. To minimize the thermal interaction between the ZBLAN fiber and the environment, the ZBLAN fiber is supported by two thin glass fibers as shown in Fig. 1(b).

The fluorescence spectral power density of the ZBLAN fiber, $S(\lambda)$, is measured from the side by a multimode optical fiber, which is coupled to a spectrometer. We note that the position of this multimode optical fiber does not change relative

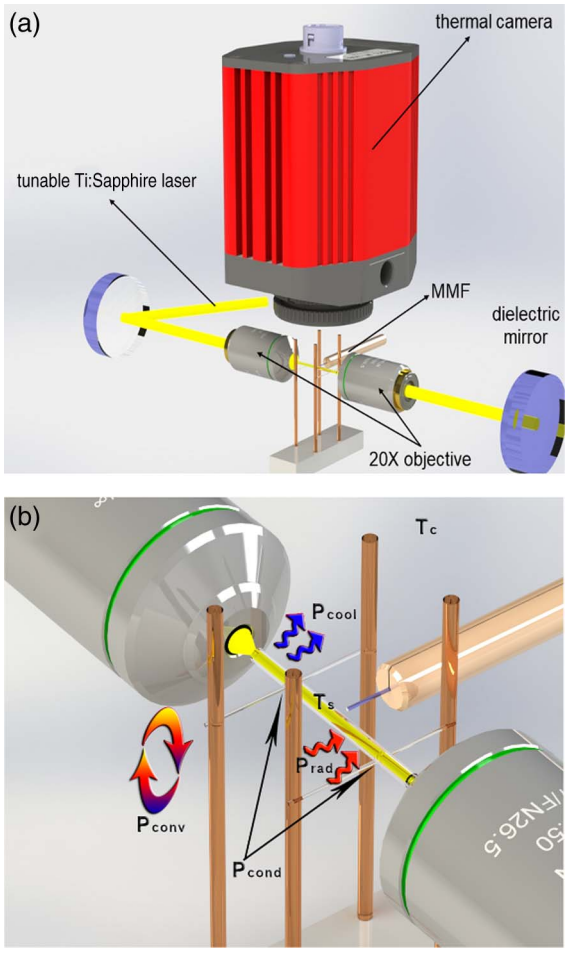

Fig. 1. (a) Experimental setup for the LITMoS test of the Yb-doped ZBLAN fiber. (b) Magnified image of the fiber holder and an illustration of the three sources of heat load: convective, conductive, and radiative.

to the ZBLAN fiber during the LITMoS test. Therefore, the absorbed power density, P_{abs}, at each pump wavelength, λ_p, is proportional to the total collected fluorescence spectral power. In other words, $P_{abs}(\lambda_p) \propto \int d\lambda S_p(\lambda)$, where the integral is performed over the entire fluorescence spectrum, and the subscript p in $S_p(\lambda)$ signifies that the fluorescence spectral power density relates to pumping the ZBLAN fiber at λ_p. We emphasize that by changing λ_p, only the overall intensity of $S_p(\lambda)$ is re-scaled and its spectral form does not change. P_{net} is proportional to the change in the temperature, ΔT, of the fiber, which is proportional to Δ(pixel) of the image captured by the thermal camera at each λ_p. Therefore, for the pump wavelength, λ_p, the cooling efficiency is approximated by $\eta_c \propto -\Delta(\text{pixel})/\int d\lambda S_p(\lambda)$.

In Fig. 2(a), the blue circles correspond to Δ(pixel) (change in the pixel value of the thermal camera image), and the red asterisks represent $\int d\lambda S_p(\lambda)$. The ratio is plotted in Fig. 2(b) and is fitted to Eq. (1), where the $-\Delta(\text{pixel})/\int d\lambda S_p(\lambda)$ ratio is renormalized by a single overall scaling factor to conform to

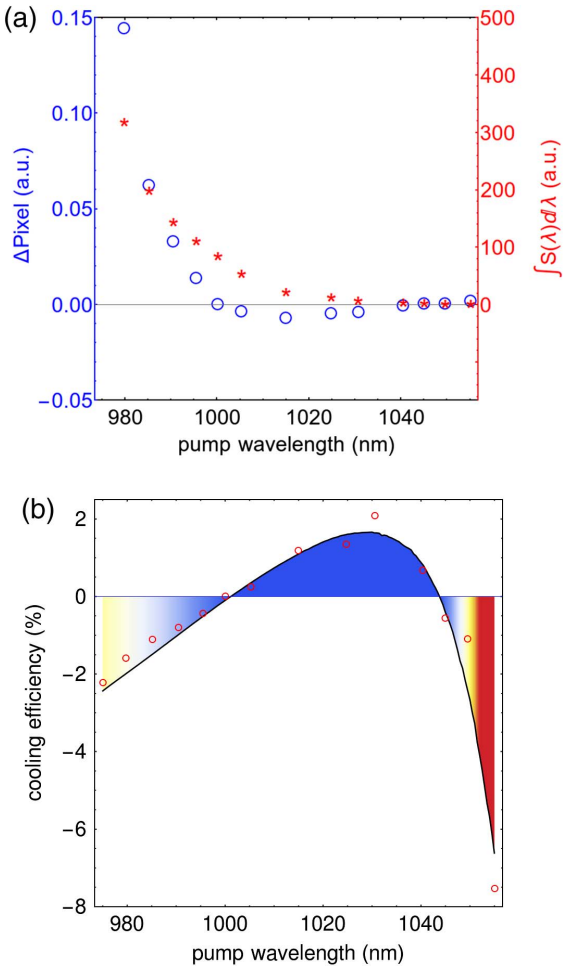

Fig. 2. (a) Blue circles correspond to Δ(pixel) (change in the pixel value of the thermal camera image) at each wavelength, and red asterisks represent the area under the $S(\lambda)$ curve. (b) Red dots represent the measurement of the cooling efficiency (η_c) for the Yb:ZBLAN fiber at different wavelengths. The solid curve shows a fitting of η_c based on Eq. (1) to the measured values, where the positive region in η_c indicates cooling.

Eq. (1). We note that $\alpha_r(\lambda_p)$ follows a strict spectral function of the form [14,23,24]

$$\alpha_r(\lambda) \propto \lambda^5 S(\lambda) \exp\left(\frac{hc}{\lambda k_B T}\right), \tag{3}$$

which is used in Eqs. (1) and (2) to perform the fit. Here, h is the Planck constant, k_B is the Boltzmann constant, c is the speed of light in vacuum, and T can be the room temperature as long as the temperature variation due to ASF cooling is not large. Equation (3) represents a proportional relationship that cannot be directly inserted into Eq. (2). Therefore, a ratio of absorption values is needed to eliminate the proportionality constant and create an equality expression that can, indeed, be inserted into Eq. (2). To do this, we replace $\alpha_r(\lambda)$ in Eq. (2) with $\alpha_r^p \times \tilde{\alpha}_r(\lambda)$, where $\tilde{\alpha}_r(\lambda)$ is the absorption coefficient normalized to its peak value, $\alpha_r^p = \alpha_r(\lambda_{peak})$. The value of the mean fluorescence wavelength, λ_f, is also directly calculated from the measured power spectral density, $S(\lambda)$. Therefore, the fitting procedure in Fig. 2(b) becomes a two-parameter fit (besides the overall scaling), to determine the ratio α_b/α_r^p and the external quantum efficiency, η_q. We find that $\alpha_b/\alpha_r^p = 2.363 \times 10^{-4}$ and $\eta_q = 99.6\%$.

3. MEASURING THE RESONANCE ABSORPTION

In the previous section, we managed to determine the external quantum efficiency, η_q, along with the ratio of the parasitic background absorption to the peak resonant absorption, α_b/α_r^p. To find the actual values of α_b and α_r^p (not just the ratio), we can now use the MACSLA method [22,25,26]. The MACSLA method is based on comparing the collected spontaneous emission power at two arbitrary points along the fiber for different pump wavelengths. For a multimode optical fiber, due to a larger Yb-doped core diameter and consequently a stronger signal from the side of the fiber, it is not necessary to use a lock-in amplifier that was detailed in Ref. [22] for a single-mode implementation. Here, we measured the spontaneous emission power directly by a power meter from the side of the fiber. Because the Yb-doped ZBLAN fiber is multimode, we used a passive multimode optical fiber to fully scramble the pump modes before coupling the pump to the core of the active fiber to improve the pump absorption efficiency.

The experimental setup is shown in Fig. 3(a), where a tunable Ti:sapphire laser beam is coupled to a multimode fiber (Infinicore 300, Corning) with the length of 3 m, and the output of the multimode fiber is butt-coupled to the ZBLAN fiber. Two other multimode fibers (M124L02, Thorlabs) are employed to collect the spontaneous emission from the side of the doped fiber at two different locations, points A and B marked by positions z_A and z_B, respectively, alongside the ZBLAN fiber. The collected side light is filtered with a 1.0-μm-long pass filter to remove the scattered pump, and the filtered collected fluorescence is measured with a sensitive power meter (S120C, Thorlabs). Figure 3(b) shows a schematic of the MACSLA method.

The power spectral density $S(\lambda)$ of the Yb-ZBLAN fiber is shown in Fig. 4(a). The inset shows the resonant absorption coefficient, which is normalized to its peak value and is

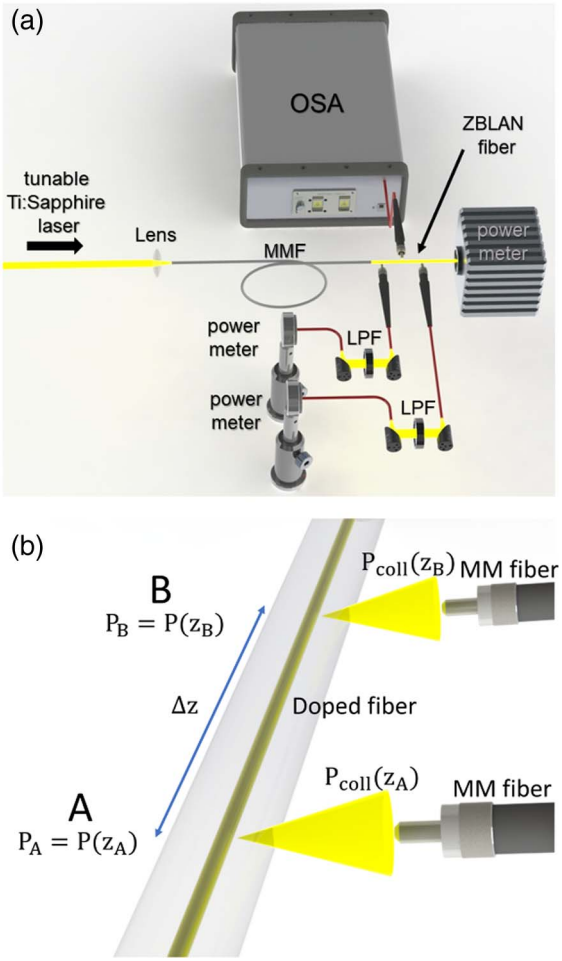

Fig. 3. (a) Schematic of the experimental setup that is used for the MACSLA method. OSA stands for optical spectrum analyzer, LPF for long-pass filter, and MMF for multimode fiber. (b) Schematic of the propagation of the pump power in the core of the optical fiber, and collection of the spontaneous emission from the side of the Yb-doped ZBLAN fiber by two multimode passive optical fibers.

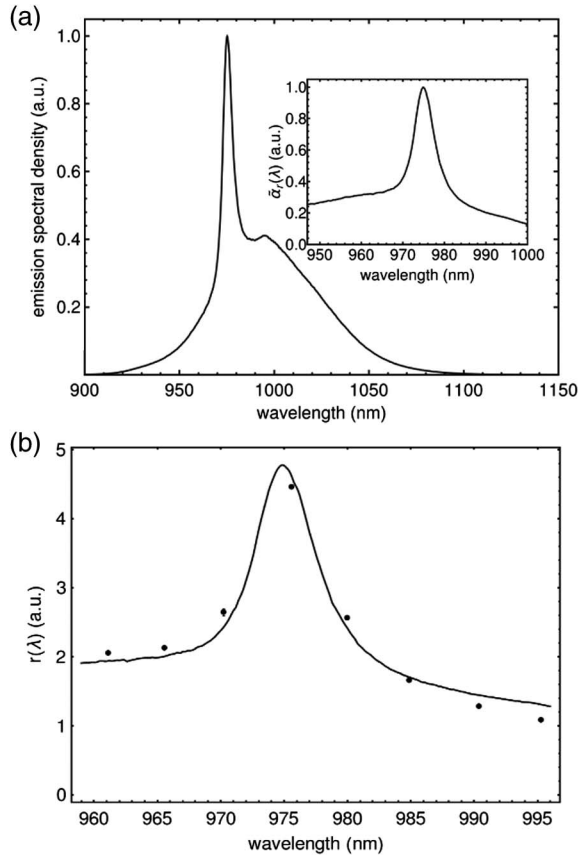

Fig. 4. (a) Emission power spectral density $S(\lambda)$, measured by the optical spectrum analyzer, is plotted in arbitrary units. The inset shows the resonant absorption coefficient, which is normalized to its peak value and is calculated by using the McCumber theory. (b) The points indicate the values of $r(\lambda)$ measured at different wavelengths near the peak of the resonant absorption coefficient.

calculated by using the McCumber theory [27]. The fitted line to the experimental measurements related to $r(\lambda) = \ln[P_{coll}(z_B)/P_{coll}(z_A)]$ is shown in Fig. 4(b). In Ref. [22], we showed that

$$r(\lambda) = \zeta - \alpha_r(\lambda)|z_B - z_A|, \tag{4}$$

where ζ is a constant here, which is unimportant for our present discussion. The points in Fig. 4(b) indicate the values of $r(\lambda)$ measured at eight different wavelengths, and the fitting curve of Eq. (4) is obtained directly from the resonant absorption spectrum shown as the inset in Fig. 4(a). The final outcome of the fitting process is the peak value of the resonant absorption coefficient, $\alpha_r^p = 1.86\ \text{cm}^{-1}$, which can be combined with the result from the LITMoS test to give $\alpha_b = 4.278 \times 10^{-2}\ \text{m}^{-1}$.

The results presented in Sections 2 and 3 amount to a detailed laser-cooling characterization of the Yb-doped ZBLAN optical fiber using the LITMoS and MACSLA methods. In particular, we have captured the wavelength dependence of the cooling efficiency η_c, the value of the external quantum efficiency η_q, the peak value and wavelength dependence of the resonance absorption coefficient $\alpha_r(\lambda)$, as well as the value of the parasitic background absorption α_b. The accurate determination of these parameters is essential for properly designing a radiation-balanced fiber laser or amplifier, an example of which will be done in the next section.

4. SIMULATION AND RESULTS

In this section, we use the experimental results on the detailed characterization of the Yb-doped ZBLAN fiber from Sections 2 and 3 to investigate the possibility of designing a viable radiation-balanced fiber laser. Our simulations are intended to highlight the possibility of designing such lasers with negligible heat production to address the laser heating and mode-instability problems. For our simulations, we use the main cooling-related parameters such as the cooling efficiency as a function of the wavelength, resonance absorption coefficient, background absorption coefficient, and the external quantum efficiency, all of which were found experimentally in the previous sections. The platform for our design is a double-cladding fiber laser geometry with two distributed Bragg reflectors on each

side of the fiber as shown in Fig. 5, which is the common platform for high-power operation.

We consider an active fiber of length L with the dopant density N, which is assumed to be constant along the fiber (independent of the position z). The pump power $P_p(z)$ at wavelength λ_p is coupled into the inner cladding at $z = 0$, propagates along the fiber, and is gradually coupled into and absorbed by the core. The unabsorbed portion of the pump that reaches the output reflector at $z = L$ is reflected back with 100% efficiency [$R_2(\lambda_p) = 1$]. For all our simulations, the reflection coefficient at the signal wavelength of the input mirror at $z = 0$ is 100%, i.e., $R_1(\lambda_s) = 1.0$. The reflection coefficient of the output coupler at the signal wavelength, i.e., $R_2(\lambda_s)$, will be optimized for the best performance in our simulations. Note that the material and dopant properties of the fiber studied for this simulation are exactly the same as the fiber characterized in the previous sections; however, its geometry is different and customized for high-power operation, as shown in Fig. 5, i.e., a single-mode core and a double-cladding geometry.

The fraction of the pump power coupled to the active core of the fiber is represented by the power filling factor Γ_p, which is assumed to be the ratio of the area of the active core to the area of the multimode inner cladding. The generated and amplified laser signal power, $P_s^{\pm}(z)$, is concentrated mainly in the core with the power filling factor (core overlap factor) Γ_s. Γ_s is the fraction of the signal power that overlaps the fiber core and is obtained by calculating the modal profile of the signal using a Gaussian profile approximation. Our analysis is based on the commonly used rate equation model for Yb-doped fibers [28]. We also consider the background absorption losses to be the same (α_b) for both the signal and the pump. For continuous wave (CW) lasers, the set of coupled time-independent steady-state rate equations and pump/signal propagation equations are given by

$$\frac{N_2(z)}{N} = \frac{\Gamma_s\sigma_s^a\lambda_s\widetilde{P}_s(z) + \Gamma_p\sigma_p^a\lambda_p\widetilde{P}_p(z)}{\Gamma_s\sigma_s^{ae}\lambda_s\widetilde{P}_s(z) + \Gamma_p\sigma_p^{ae}\lambda_p\widetilde{P}_p(z) + hcA\tau^{-1}}, \tag{5}$$

$$\pm\frac{dP_p^{\pm}}{dz} = -\Gamma_p[\sigma_p^a N - \sigma_p^{ae}N_2(z)]P_p^{\pm}(z) - \alpha_b P_p^{\pm}(z), \tag{6}$$

$$\pm\frac{dP_s^{\pm}}{dz} = -\Gamma_s[\sigma_s^a N - \sigma_s^{ae}N_2(z)]P_s^{\pm}(z) - \alpha_b P_s^{\pm}(z), \tag{7}$$

where we have used the following definitions:

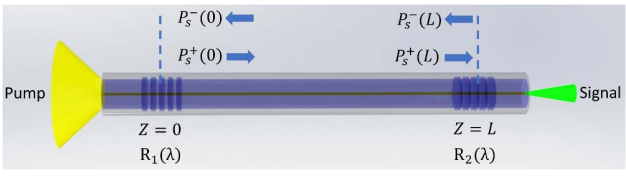

Fig. 5. Schematic of the laser system and propagation of the pump power and signal in the double-cladding fiber laser. Pump power is launched at $z = 0$, and the output signal is calculated at $z = L$ at the power delivery port. $R_1(\lambda)$ and $R_2(\lambda)$ are the distributed Bragg reflectors at $z = 0$ and $z = L$.

$$\widetilde{P}_s(z) \coloneqq P_s^+(z) + P_s^-(z), \qquad \sigma_s^{ae} \coloneqq \sigma_s^a + \sigma_s^e,$$
$$\widetilde{P}_p(z) \coloneqq P_p^+(z) + P_p^-(z), \qquad \sigma_p^{ae} \coloneqq \sigma_p^a + \sigma_p^e. \tag{8}$$

Here, $N_2(z)$ is the upper manifold population, which varies along the fiber, N is the total Yb^{3+} concentration, λ_s (λ_p) is the signal (pump) wavelength, σ_s^a (σ_p^a) is the absorption cross section at the signal (pump) wavelength, σ_s^e (σ_p^e) is the emission cross section at signal (pump) wavelength, τ is the upper manifold lifetime, and A is the cross-sectional area of the core. The $\pm$ superscripts and coefficients in the pump and signal power propagation equations signify the positive and negative propagation directions, respectively. We have used the values of the parameters reported in Table 1 in our simulations. The value of Yb^{3+} concentration in Table 1 is consistent with our measured value of α_r.

To achieve the anti-Stokes fluorescence cooling (and consequently the RBL condition), the laser must be pumped at a wavelength longer than the mean fluorescence wavelength ($\lambda_p > \lambda_f$). We measured the λ_f in our Yb-doped ZBLAN fiber sample to be 994.96 nm. In conventional fiber lasers, the fiber is pumped at the wavelength corresponding to the peak of the absorption, which is approximately 975 nm. For the RBL design, the pump wavelength is considerably longer at which the pump absorption coefficient is significantly reduced. Therefore, the optimum design parameters for an RBL system, specifically L and $R_2(\lambda_s)$, would have to be quite different from that of a conventional fiber laser. An important metric for the performance of a high-power laser is its efficiency; therefore, we compare the maximum efficiency achievable by the laser system obtained for different values of the pump wavelength, λ_p, and signal wavelength, λ_s.

Figure 6 shows a density plot of the optimum efficiency as a function of the pump and signal wavelengths. The efficiency is defined as the output signal power divided by the input pump power. At every point in Fig. 6 identified by a (λ_p, λ_s) pair, we run an optimization code to find the length L and the output

Table 1. Yb-Doped ZBLAN Fiber Simulation Parameters

Symbol	Parameter	Value
d_{co}	Core diameter	6.5 μm
d_{cl}	Cladding diameter	125 μm
Γ_s	Signal power filling factor	0.89
Γ_p	Pump power filling factor	2.704×10^{-3}
N	Yb^{3+} concentration	1.453×10^{26} m^{-3}
τ	Upper manifold lifetime	1.7 ms
H	Convective heat transfer coefficient	30 $W/(m^2 \cdot K)$
σ_{abs} (975 nm)	Absorption cross section	1.28×10^{-24} m^{-2}
σ_{em} (975 nm)	Emission cross section	1.28×10^{-24} m^{-2}
λ_f	Mean fluorescence wavelength	994.96 nm
α_b	Background absorption (pump & signal)	4.278×10^{-2} m^{-1}
η_q	External quantum efficiency	99.6%
$R_2(\lambda_p)$	Pump reflection of output mirror	100%
$R_1(\lambda_s)$	Signal reflection of input mirror	100%

signal reflectivity $R_2(\lambda_s)$ corresponding to the maximum achievable output signal power for 80 W of input pump power. Therefore, the efficiency at each point is the maximum value that is achievable in a system design. Of course, the values of L and $R_2(\lambda_s)$ can be widely different at different points in Fig. 6. For example, the optimum length and reflectivity for $\lambda_p = 1035$ nm and $\lambda_s = 1080$ nm are 24.1 m and 30%, but the same parameters for $\lambda_p = 940$ nm and $\lambda_s = 1060$ nm are 8.2 m and 4%. Figure 6 provides a powerful comparison of the maximum achievable efficiencies at different wavelengths, where one does not need to worry about whether the lower efficiency is because of the choice of the wavelengths or because of the non-optimal choice of the fiber length and output reflectivity.

According to the results presented in Fig. 6, the maximum efficiency of around 70% is obtained for the pump wavelength of around 975 nm, which corresponds to the peak of the absorption cross section of the Yb-doped ZBLAN. In RBL systems, the pump wavelength is typically longer than 1020 nm. The inset in Fig. 6 is a magnification of the density plot over the range of wavelengths, which are most relevant for an RBL design. It can be seen that a range of 5%–10% efficiency is the best that can be achieved in the Yb-doped ZBLAN fiber explored here. These general observations persist for any Yb-doped optical fiber in an RBL design, which inevitably falls in the low efficiency region in Fig. 6, because the pump wavelength must be longer than 1020 nm. Therefore, the only reasonable justification for such a design can be when one must sacrifice the maximum achievable efficiency for the better heat management or even the total heat mitigation in a strict RBL system.

Now that we have an account of the maximum achievable efficiency from Fig. 6, we still need to answer the key question for an RBL system design: is it possible to have a fiber RBL with the same output power as a conventional fiber laser, and with the additional benefit of generating little or no heat? This is the central question in designing a meaningful fiber RBL. To explore it, we consider two simulations: first for a conventional fiber laser pumped at $\lambda_p = 975$ nm presented in Fig. 7(a), and second for a radiation-balanced fiber laser pumped at $\lambda_p = 1030$ nm presented in Fig. 7(b). The output signal in both lasers is generated to be at $\lambda_s = 1070$ nm and is 3 W in power. Both systems are optimized for maximum efficiency. Of course, for the conventional fiber laser corresponding to Fig. 7(a), the required pump power is only 4.68 W because of the higher efficiency. However, for the RBL design, we need 78 W of input pump power to achieve 3 W of output signal power due to the lower efficiency. In each plot, we show the temperature rise (ΔT) as a function of z along the fiber. It can be seen that the temperature rise in both designs is comparable, and the RBL design even runs slightly hotter; although the RBL design is pumped at a wavelength at which ASF cooling is mitigating some of the generated heat, its lower efficiency is resulting in more temperature rise. This means that we cannot obtain any meaningful design because the best we can achieve is a comparable temperature rise, albeit with a substantially higher pump power. Therefore, an RBL design cannot be justified. We note that the value of α_b that we measured earlier for the ZBLAN fiber for signal propagating in the core appears to be somewhat high, most likely due to the age of the sample (>10 years) and exposure to moisture and oxygen (room storage) [29–31]. The measured attenuation in our fiber is less than 0.19 dB/m, while attenuation values as low as 0.01 dB/m or even lower are reported in the literature [19,32]. For the simulations presented in Fig. 7, we assume that the contribution of

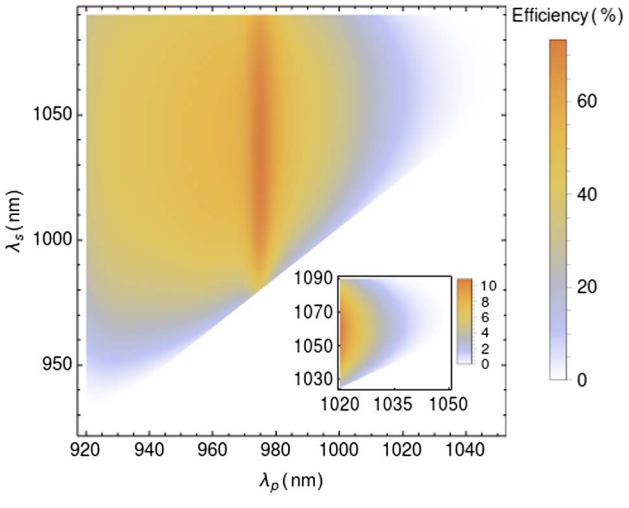

Fig. 6. Density plot of the optimum efficiency of the fiber laser for different pump and signal wavelengths, when the laser is pumped with 80 W of input pump power. The inset is a magnification of the density plot over the range of wavelengths, which are most relevant for an RBL system.

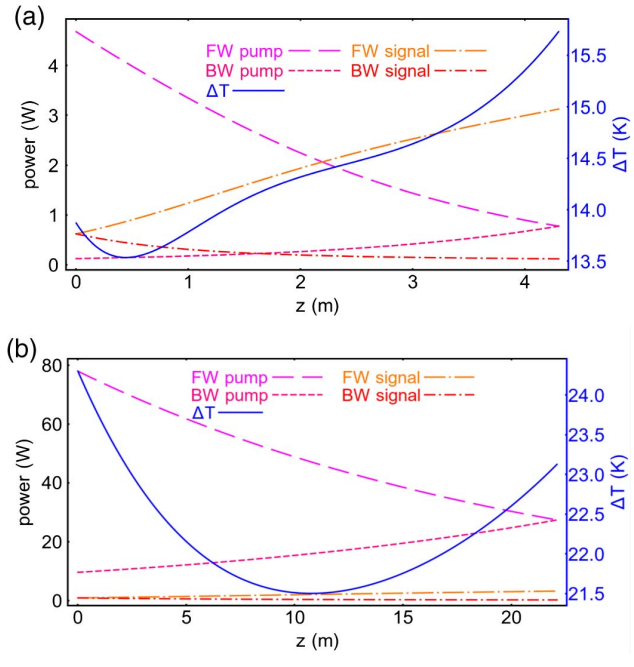

Fig. 7. (a) Propagation of the forward pump (FW pump), backward pump (BW pump), forward signal (FW signal), backward signal (BW signal), and temperature rise along the ZBLAN fiber for a conventional fiber laser pumped at $\lambda_p = 975$ nm. (b) Similar graph for the RBL operation pumped at $\lambda_p = 1030$ nm. Both lasers are optimized for the signal output power of 3 W at $\lambda_s = 1070$ nm for α_b from Table 1. Note that the fiber in the RBL design is considerably longer than in the conventional design.

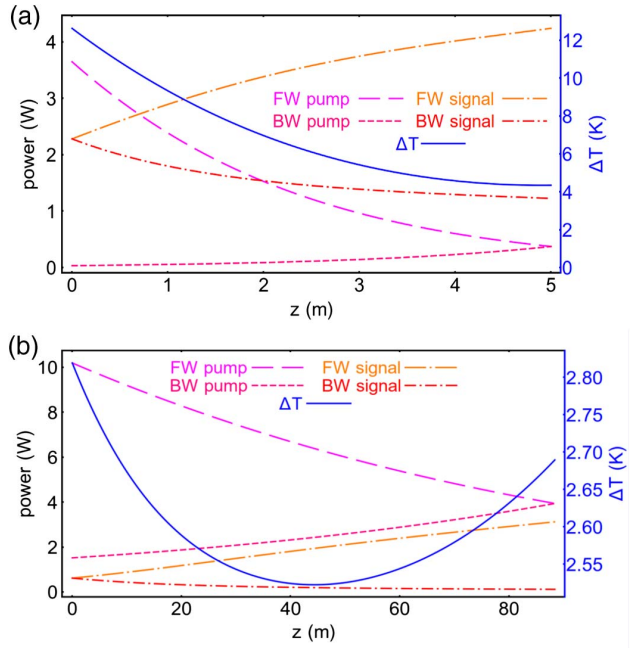

Fig. 8. Similar to Fig. 7, except the ZBLAN fiber is chosen with a 10-fold reduction in the background absorption, i.e., $\alpha_b' = \alpha_b/10$, while maintaining the parasitic absorption of 0.01 dB/m in the cladding. The reduced value is used for both the conventional laser in (a), pumped with 3.65 W at $\lambda_p = 975$ nm; and the RBL laser in (b), pumped with 10.2 W at $\lambda_p = 1030$ nm. Both lasers are optimized for the signal output power of 3 W at $\lambda_s = 1070$ nm. The RBL design has a substantially reduced temperature performance compared with the conventional laser and the trade-off of a nearly two-fold increase in the required pump power.

the parasitic absorption to the total attenuation in the cladding is 0.01 dB/m, which is the amount that is responsible for heating in the cladding.

We have identified the large value of the background absorption α_b, as shown in Table 1, to be the root cause of making such RBL designs pointless, as shown in Fig. 7. Therefore, the key to achieving a viable RBL system is to lower the value of the parasitic background absorption, which should be tackled by the proper fabrication and composition of the glass. To support this argument, we have repeated the simulation presented in Fig. 7 with a 10-fold reduction in the background absorption, i.e., $\alpha_b' = \alpha_b/10$ [19]. We maintain the same level of parasitic absorption of 0.01 dB/m in the cladding. After optimizing the cavity and finding the best reflector and length of the fiber for 3 W of the output signal power, we show the designs in Fig. 8. Figure 8(a), which corresponds to the conventional laser, is slightly cooler than the design in Fig. 7(a); however, the RBL design in Fig. 8(b) shows a much smaller temperature rise compared with Fig. 7(b), hence confirming our claim.

5. DISCUSSION AND CONCLUSION

Anti-Stokes fluorescence cooling and radiation-balancing of fiber lasers and amplifiers rely on the availability of cooling-grade rare-earth-doped optical fibers. Herein, we have performed a detailed investigation of an Yb-doped ZBLAN optical fiber to assess its gain, loss, and cooling-related parameters. The techniques are based on the LITMoS test developed in Sheik-Bahae's research group and the MACSLA method recently developed in our group, and they give accurate results on the cooling behavior of the Yb-doped ZBLAN fiber. A main advantage of the MACSLA method is that unlike the cutback method, it is not destructive. We emphasize that this work constitutes the first such detailed assessment of a cooling-grade optical fiber over a range of wavelengths. More importantly, the entire measurement is performed at atmospheric pressure using conventional table-top optical equipment. It is shown that the specific ZBLAN fiber sample measured in the experiments is cooling grade. However, its parasitic background absorption is too large to be used for proper radiation balancing in a fiber laser or amplifier design.

As it is shown in Fig. 6, the maximum efficiency for our Yb-doped ZBLAN fiber is obtained when it is pumped around 975 nm wavelength, while the efficiency of the laser at favorable wavelengths for RBL operation ($\lambda_p \gtrsim 1020$ nm) is ~7 times smaller. This lower efficiency is mainly due to the smaller absorption cross section of the pump power at RBL pump wavelengths. To assess the viability of an RBL design, we compared a conventional laser pumped at 975 nm wavelength with an RBL design pumped at $\lambda_p = 1030$ nm (see Fig. 7). The output signal in both lasers was assumed to be 3 W in power at $\lambda_s = 1070$ nm, and both systems were optimized for maximum efficiency (fiber length and output signal reflectivity). We observed that the temperature rise in both designs was comparable, while the RBL design required a 20-fold larger pump power, making the RBL design totally unpractical. We attributed the problem to the relatively large value of the parasitic absorption of the pump α_b; in a separate simulation in Fig. 8, we showed that a 10-fold reduction in α_b can reduce the heating in the RBL design significantly and make it viable. Therefore, we conclude that the key to achieving a viable RBL design in optical fibers is to focus on the fabrication and composition of the glass to reduce α_b. For fiber lasers, because the parasitic heat is proportional to α_b and the pump/signal powers, and the cooling happens only in the core while the parasitic heating happens both in the core and the cladding, the demand on reducing α_b is higher than other forms of RBL lasers [33]. In fact, our analysis has shown that while the value of α_b is small enough to make our sample a cooling-grade fiber, it is not sufficiently small to make it a viable gain medium for RBL operation. Therefore, as far as fiber lasers are concerned, a viable RBL laser is more demanding on the parasitic absorption coefficient than the laser-cooling experiment. We note that we have not included amplified spontaneous emission (ASE) in our simulation, because its inclusion likely amounts to negligible changes in our results [20]. However, we intend to include ASE in our future simulations that are meant to target system designs.

APPENDIX A: DERIVATION OF THE COOLING EFFICIENCY FORMULA

The cooling efficiency, η_c, is defined as the net power density (per unit volume) extracted from the material (P_{net}) per unit power density absorbed or scattered (P_{abs}): $\eta_c = P_{\text{net}}/P_{\text{abs}}$.

We can write $P_{\text{net}} = P_{\text{asf}} - P_{\text{abs}}$, where P_{asf} is the fraction of the ASF power density that escapes the cooling material. The absorbed power density is given by $P_{\text{abs}} = (\alpha_r + \alpha_b)I_P$, where I_P is the pump intensity, α_r is the resonant absorption of the pump laser due to the presence of the gain materials (Yb ions here), and α_b represents the parasitic background absorption and scattering of the pump laser. The ASF power density is therefore given by $\eta_e N_2 W_r(h\nu_f)$, where ν_f is the mean fluorescence frequency, N_2 is the number density of the excited upper level in the quasi two-level Yb ions, and W_r (W_{nr}) is the radiative (non-radiative) decay rate of the excited state of the doped ions. η_e is the extraction (escape) efficiency, and $1-\eta_e$ is the fraction of photons that are radiated but are trapped inside the host. The rate equation can be expressed as

$$\frac{dN_2}{dt} = \frac{\alpha_r I_P}{h\nu_p} - (W_r + W_{nr})N_2 + (1-\eta_e)W_r N_2, \quad \textbf{(A1)}$$

where we have assumed that the trapped fluorescence is reabsorbed by the Yb ions. In steady state, where $dN_2/dt = 0$, we can solve for N_2 and obtain $P_{\text{asf}} = \alpha_r I_P \eta_q(\lambda_p/\lambda_f)$, where the external quantum efficiency is given by $\eta_q = \eta_e W_r/(\eta_e W_r + W_{nr})$, and λ_p (λ_f) is the pump (mean fluorescence) wavelength. We therefore have

$$P_{\text{net}} = (\alpha_r + \alpha_b)I_P - \alpha_r I_P \eta_q(\lambda_p/\lambda_f). \quad \textbf{(A2)}$$

We can use these results to present the cooling efficiency in the form of Eq. (1).

APPENDIX B: COOLING GRADE POLISHING OF THE ZBLAN FIBER

The laser cooling and LITMoS test are very sensitive to surface impurities: dust particles, contamination, or scratches on the fiber facets, which act as sources of external heating and can negatively impact the laser-cooling experiment. Therefore, high-quality polishing and cleaning of the optical fiber facets are critical steps for a successful LITMoS experiment [9,34]. ZBLAN fibers are made from a soft glass, which is prone to oxidation; therefore, it is much harder to polish their facets to a high-quality finish compared with silica fibers. Moreover, commercial equipment for polishing and processing ZBLAN fibers is not as widely available as for silica fibers. In this section, we detail the procedure we followed to polish our ZBLAN fiber for the laser-cooling experiment.

To begin the polishing process, as it is shown in Fig. 9(a), we placed the fiber on a home-made polishing fixture, which is made of stainless steel. The choice of a stainless steel polishing fixture is crucial because the aluminum oxide that forms on an aluminum fixture can easily delaminate during the polishing procedure and can scratch the fiber facet. We heated Crystalbond 509 and used it to glue the fiber at its position in the polishing fixture. The fiber and Crystalbond were then polished with a 30 μm grit polishing sheet. As it is shown in Fig. 9(b), this procedure continues until the full circular shape of the core cladding of the facet of the fiber appears under the microscope. We followed a wet polishing procedure and used water-free glycol and glycerin combination for the liquid element because ZBLAN interacts with oxygen and OH. The polishing procedure continued with polishing sheets of 5, 3, 1, 0.3, and 0.02 μm grits, sequentially. After each step, the facet of fiber was inspected under a microscope, and if there was a scratch, we repeated the previous steps. The final surface of the doped ZBLAN fiber is shown in the last image of Fig. 9(c).

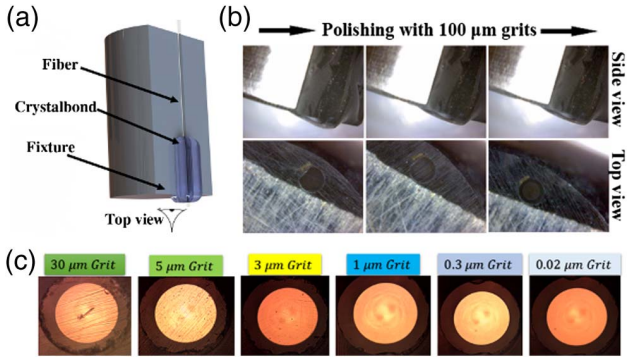

Fig. 9. (a) Images of the polishing fixture and the ZBLAN doped fiber, which are glued together by the Crystalbond. (b) Initial coarse polishing steps to prepare a flat surface for further polishing. From left to right, the side and facet views of the doped fiber are shown for each step of the coarse polishing. (c) Images of the facet of the ZBLAN fiber under microscope after each fine-polishing step.

Cleaning the facets is another crucial step in fiber preparation. The cleaning is done immediately after the fiber is polished. The fiber and the polishing fixture are immersed in a 99.5% acetone solution in an ultrasound bath for about 30 min for dissolving the bulk Crystalbond and detaching the fiber from the polishing fixture. The fiber is then soaked in a Citrosolve solution in the ultrasound bath to dissolve the residual Crystalbond for about 1 h. The fiber is then dipped in a 99.5% acetone solution for about 4 h to clean the fiber thoroughly. Following this, the fiber is immersed in the 99.999% isopropanol for 30 min in the ultrasound bath to clean any trace of acetone. To emphasize the importance of such a cooling-grade polishing procedure, in Fig. 10(a), we show the thermal camera images of the ZBLAN fiber that is pumped at the 1030 nm wavelength. The three images show, sequentially, that

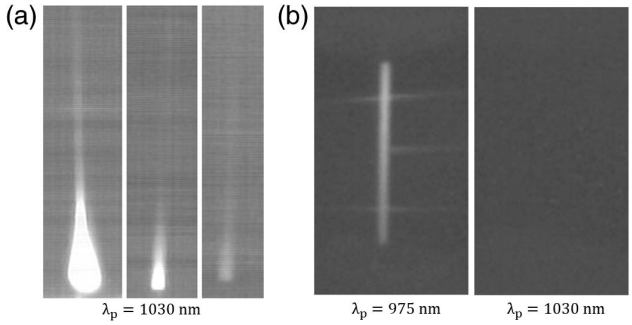

Fig. 10. Thermal camera images of the laser-pumped ZBLAN fiber. Images in subfigure (a) are for pumping at the 1030 nm wavelength and sequentially improved polishing of the facets. The brighter spots indicate heating, and as the polishing quality is improved, the facet heating is reduced. When cooling-grade polishing is reached, the facets no longer are sources of parasitic heating in subfigure (b), and transition from heating to cooling is clearly observed when the pump wavelength is switched from 975 to 1030 nm wavelength.

the improved polishing of the facets results in reduced heating of the facets. In Fig. 10(b) where the fiber is highly polished and the facets no longer are sources of parasitic heating, one can clearly observe the transition from heating when the fiber is pumped at 975 nm wavelength to cooling when pumped at 1030 nm wavelength.

Funding. This material is based upon work supported by the Air Force Office of Scientific Research under award number FA9550-16-1-0362 titled Multidisciplinary Approaches to Radiation Balanced Lasers (MARBLE).

Acknowledgment. The authors would like to acknowledge M. Sheik-Bahae, R. I. Epstein, M. P. Hehlen, M. Hossein-Zadeh, and A. R. Albrecht for informative discussions.

Disclosures. The authors declare no conflicts of interest.

REFERENCES

1. D. J. Richardson, J. Nilsson, and W. A. Clarkson, "High power fiber lasers: current status and future perspectives [invited]," J. Opt. Soc. Am. B **27**, B63–B92 (2010).
2. M. N. Zervas and C. A. Codemard, "High power fiber lasers: a review," IEEE J. Sel. Top. Quantum Electron. **20**, 219–241 (2014).
3. D. C. Brown and H. J. Hoffman, "Thermal, stress, and thermo-optic effects in high average power double-clad silica fiber lasers," IEEE J. Quantum Electron. **37**, 207–217 (2001).
4. L. Zenteno, "High-power double-clad fiber lasers," J. Lightwave Technol. **11**, 1435–1446 (1993).
5. B. Ward, C. Robin, and I. Dajani, "Origin of thermal modal instabilities in large mode area fiber amplifiers," Opt. Express **20**, 11407–11422 (2012).
6. J. W. Dawson, M. J. Messerly, R. J. Beach, M. Y. Shverdin, E. A. Stappaerts, A. K. Sridharan, P. H. Pax, J. E. Heebner, C. W. Siders, and C. Barty, "Analysis of the scalability of diffraction-limited fiber lasers and amplifiers to high average power," Opt. Express **16**, 13240–13266 (2008).
7. C. Jauregui, T. Eidam, H.-J. Otto, F. Stutzki, F. Jansen, J. Limpert, and A. Tünnermann, "Physical origin of mode instabilities in high-power fiber laser systems," Opt. Express **20**, 12912–12925 (2012).
8. R. I. Epstein, M. I. Buchwald, B. C. Edwards, T. R. Gosnell, and C. E. Mungan, "Observation of laser-induced fluorescent cooling of a solid," Nature **377**, 500–503 (1995).
9. D. V. Seletskiy, S. D. Melgaard, S. Bigotta, A. Di Lieto, M. Tonelli, and M. Sheik-Bahae, "Laser cooling of solids to cryogenic temperatures," Nat. Photonics **4**, 161–164 (2010).
10. S. R. Bowman, "Lasers without internal heat generation," IEEE J. Quantum Electron. **35**, 115–122 (1999).
11. S. R. Bowman, S. P. O'Connor, S. Biswal, N. J. Condon, and A. Rosenberg, "Minimizing heat generation in solid-state lasers," IEEE J. Quantum Electron. **46**, 1076–1085 (2010).
12. S. R. Bowman, "Low quantum defect laser performance," Opt. Eng. **56**, 011104 (2016).
13. Z. Yang, J. Meng, A. R. Albrecht, and M. Sheik-Bahae, "Radiation-balanced Yb:YAG disk laser," Opt. Express **27**, 1392–1400 (2019).
14. E. Mobini, M. Peysokhan, B. Abaie, M. P. Hehlen, and A. Mafi, "Spectroscopic investigation of Yb-doped silica glass for solid-state optical refrigeration," Phys. Rev. Appl. **11**, 014066 (2019).
15. C. Mungan, M. Buchwald, B. Edwards, R. Epstein, and T. Gosnell, "Laser cooling of a solid by 16 K starting from room temperature," Phys. Rev. Lett. **78**, 1030–1033 (1997).
16. X. Luo, M. D. Eisaman, and T. R. Gosnell, "Laser cooling of a solid by 21 K starting from room temperature," Opt. Lett. **23**, 639–641 (1998).
17. T. Gosnell, "Laser cooling of a solid by 65 K starting from room temperature," Opt. Lett. **24**, 1041–1043 (1999).
18. A. Rayner, M. Hirsch, N. R. Heckenberg, and H. Rubinsztein-Dunlop, "Distributed laser refrigeration," Appl. Opt. **40**, 5423–5429 (2001).
19. J. Knall, A. Arora, M. Bernier, S. Cozic, and M. J. F. Digonnet, "Demonstration of anti-Stokes cooling in Yb-doped ZBLAN fibers at atmospheric pressure," Opt. Lett. **44**, 2338–2341 (2019).
20. E. Mobini, M. Peysokhan, B. Abaie, and A. Mafi, "Thermal modeling, heat mitigation, and radiative cooling for double-clad fiber amplifiers," J. Opt. Soc. Am. B **35**, 2484–2493 (2018).
21. S. Melgaard, D. Seletskiy, V. Polyak, Y. Asmerom, and M. Sheik-Bahae, "Identification of parasitic losses in Yb:YLF and prospects for optical refrigeration down to 80 K," Opt. Express **22**, 7756–7764 (2014).
22. M. Peysokhan, E. Mobini, B. Abaie, and A. Mafi, "Method for measuring the resonant absorption coefficient of rare-earth-doped optical fibers," Appl. Opt. **58**, 1841–1846 (2019).
23. T. Newell, P. Peterson, A. Gavrielides, and M. Sharma, "Temperature effects on the emission properties of Yb-doped optical fibers," Opt. Commun. **273**, 256–259 (2007).
24. B. Aull and H. Jenssen, "Vibronic interactions in Nd: Yag resulting in nonreciprocity of absorption and stimulated emission cross sections," IEEE J. Quantum Electron. **18**, 925–930 (1982).
25. M. Peysokhan, E. M. Souchelmaei, B. Abaie, and A. Mafi, "A non-destructive method for measuring the absorption coefficient of a doped optical fiber," Proc. SPIE **10936**, 109360K (2019).
26. M. Peysokhan, E. Mobini, B. Abaie, and A. Mafi, "A non-destructive method for measuring the absorption coefficient of a Yb-doped fiber," in *Laser Science* (Optical Society of America, 2018), paper JW3A–138.
27. D. McCumber, "Einstein relations connecting broadband emission and absorption spectra," Phys. Rev. **136**, A954–A957 (1964).
28. I. Kelson and A. A. Hardy, "Strongly pumped fiber lasers," IEEE J. Quantum Electron. **34**, 1570–1577 (1998).
29. H. Malik and K. Maqsood, "Effect of distilled water on the optical properties and surface degradation of Zr-Ba based glass," J. Mater. Sci. **37**, 5367–5369 (2002).
30. A. P. Rizzato, C. V. Santilli, S. H. Pulcinelli, Y. Messaddeq, and P. Hammer, "XPS study of the corrosion protection of fluorozirconate glasses dip-coated with SnO_2 transparent thin films," J. Sol-Gel Sci. Technol. **32**, 155–160 (2004).
31. A. P. Rizzato, C. V. Santilli, S. H. Pulcinelli, Y. Messaddeq, A. F. Craievich, and P. Hammer, "Study on the initial stages of water corrosion of fluorozirconate glasses," J. Non-Cryst. Solids **348**, 38–43 (2004).
32. X. Zhu and N. Peyghambarian, "High-power ZBLAN glass fiber lasers: review and prospect," Adv. OptoElectron. **2010**, 501956 (2010).
33. E. Mobini, M. Peysokhan, and A. Mafi, "Heat mitigation of a core/cladding Yb-doped fiber amplifier using anti-Stokes fluorescence cooling," J. Opt. Soc. Am. B **36**, 2167–2177 (2019).
34. M. Peysokhan, B. Abaie, E. Mobini, S. Rostami, and A. Mafi, "Measuring quantum efficiency and background absorption of an ytterbium-doped ZBLAN fiber," in *CLEO: Applications and Technology* (Optical Society of America, 2018), paper JW2A–118.